

Metal ions-binding T4 lysozyme as an intramolecular protein purification tag compatible with X-ray crystallography

Evzen Boura, Adriana Baumlova, Dominika Chalupska, Anna Dubankova, and Martin Klima*

Institute of Organic Chemistry and Biochemistry, Czech Academy of Sciences, Prague, Czech Republic

Received 11 January 2017; Accepted 17 March 2017

DOI: 10.1002/pro.3162

Published online 25 March 2017 proteinscience.org

Abstract: Phage T4 lysozyme is a well folded and highly soluble protein that is widely used as an insertion tag to improve solubility and crystallization properties of poorly behaved recombinant proteins. It has been used in the fusion protein strategy to facilitate crystallization of various proteins including multiple G protein-coupled receptors, lipid kinases, or sterol binding proteins. Here, we present a structural and biochemical characterization of its novel, metal ions-binding mutant (mbT4L). We demonstrate that mbT4L can be used as a purification tag in the immobilized-metal affinity chromatography and that, in many respects, it is superior to the conventional hexahistidine tag. In addition, structural characterization of mbT4L suggests that mbT4L can be used as a purification tag compatible with X-ray crystallography.

Keywords: phage T4; lysozyme; endolysin; histidine tag; protein purification; crystal structure

Introduction

The lysozyme of enterobacteria phage T4 (also known as endolysin, muramidase, hereafter referred to as T4 lysozyme) is a protein capable of degradation of host peptidoglycans by hydrolysis of the linkages between *N*-acetylmuramic acid and

N-acetylglucosamine residues. It participates with a second lysis factor, a small membrane protein designated as holin, in the sequential events which lead to the host cell lysis releasing the mature viral particles.¹

T4 lysozyme is a well folded soluble protein that crystallizes under many different conditions.² In biochemistry and structural biology, it has served as a model molecule for studying the factors that determine the structure and stability of proteins.² Recently, it has been used in the fusion protein strategy to facilitate crystallization of various proteins including multiple G protein-coupled receptors,^{3–12} sterol binding proteins,^{13,14} or type II phosphatidylinositol 4-kinases.^{15–17} In this strategy, usually the flexible intracellular loops of the target proteins are replaced by T4 lysozyme, nevertheless, fusing T4 lysozyme to the amino terminus of the target protein could also facilitate crystallogenesis.¹⁸ A remarkable feature of T4 lysozyme is its tolerance of changes in the amino acid sequence.² The enzymatic activity is preserved upon single substitutions of more than half of the amino acid residues of T4 lysozyme.¹⁹

Statement for a broader audience: Protein tags are peptide sequences genetically grafted onto a recombinant protein to improve its properties, e.g., in terms of specific affinity or solubility. In this study, we present a structural and biochemical characterization of a novel intramolecular protein purification tag derived from enterobacteria phage T4 lysozyme and we investigate its utilization in the immobilized-metal affinity chromatography.

Grant sponsor: Czech Science Foundation; Grant number: 17-07058Y; Grant sponsor: Academy of Sciences of the Czech Republic; Grant number: RVO: 61388963; Grant sponsor: Ministry of Education, Youth and Sports of the Czech Republic; Grant number: LO1302 - InterBioMed.

*Correspondence to: Martin Klima, Institute of Organic Chemistry and Biochemistry, Czech Academy of Sciences, Flemingovo namesti 2, 166 10 Prague 6, Czech Republic. E-mail: klima@uochb.cas.cz

In this study, we present a structural and biochemical characterization of its novel, metal ions-binding mutant (mbT4L). Specifically, we present a crystal structure of mbT4L in complex with Ni²⁺ ions at resolution of 1.8 Å. In addition, we show that mbT4L can be utilized as an intramolecular purification tag of recombinant proteins in the immobilized-metal affinity chromatography (IMAC). Compared to the commonly used *N*-terminal hexahistidine tag, mbT4L is not affected by degradation of the intrinsically disordered *N*-termini of the target proteins resulting in their higher yields, binds to the immobilized metal ions with stronger affinity resulting in higher purity of purified proteins, and improves the solubility of the target proteins. In addition, upon crystallization of the mbT4L-fusion protein the anomalous signal of the bound metal ions may be utilized for phasing along with the known structure of the mutant lysozyme. Taken together, our data provide a structural rationale for a novel intramolecular protein purification tag compatible with both the IMAC and X-ray crystallography techniques.

Results

Design and crystal structure of the metal ions-binding T4 lysozyme

Wild type T4 lysozyme (wtT4L) is composed of an *N*-terminal alpha helix α 1, *N*-terminal lobe formed by three beta strands β 1- β 3 and one alpha helix α 2, and a *C*-terminal lobe formed by nine alpha helices α 3- α 11 [Fig. 1(A,B)]. The substrate binding groove is located between the lobes.²² The flexibility between the lobes is required for the enzymatic activity of T4 lysozyme,²³ nevertheless, in some cases it may contribute to poor crystal quality of T4L-fusion proteins.²⁰

To design a protein with desired properties, we choose truncated T4 lysozyme (trT4L) as described by Thorsen et al.²⁰ as our starting molecule [Fig. 1(A)]. In this “minimal version” of T4 lysozyme, the flexible *N*-terminal lobe (residues R12 to K60) is replaced with a short glycine/serine linker (-GGSGG-), which leads to the enzymatic inactivity of the trT4 lysozyme along with a limited flexibility and improved crystallization properties of the mutant protein.

To generate a metal ions-binding mutant of T4 lysozyme (mbT4L), several point mutations to trT4 lysozyme were introduced. The commonly used metal ions-binding protein purification tags usually contain 6-10 histidines which are sterically capable of forming coordinate covalent bonds with metal ions such as Co²⁺, Cu²⁺, Ni²⁺, or Zn²⁺.²⁴ Therefore, we decided to introduce at least six to-histidine point mutations to trT4 lysozyme. The candidate amino acid residues for mutagenesis had to meet several criteria as follows: they should be solvent accessible (preferentially surface-exposed polar residues), they

should be located distally to the *N*- and *C*- termini of the molecule (preferentially within the α 7 and α 8 helices of trT4 lysozyme) to facilitate a subsequent utilization of the mutant lysozyme in the fusion protein strategy, and they should be sterically capable of forming coordinate covalent bonds with the metal ions. Homology modeling of T4L mutants based on a previously known T4L structure (PDB entry 3FA0²¹) suggested that the suitable candidates for mutagenesis could be the residues N73, R76, Q80, R82, E85, and N89 [Fig. 1(A)]. In addition to these to-histidine mutations we introduced an M77A mutation to prevent the methionine sidechain from sterical interference with the coordinate covalent bonds formed by metal ions and introduced histidines. The resulting construct was expressed in *E. coli* at high levels and could be purified to homogeneity using a simple immobilized-metal (Ni²⁺) affinity chromatography.

To evaluate the effect of the T4 lysozyme truncation combined with the mutagenesis mentioned above, we determined the structure of the mbT4L protein in complex with the nickel ions using protein crystallography. We obtained crystals that diffracted to 1.8 Å and belonged to the orthorhombic P2₁2₁2₁ space group with two molecules per asymmetric unit. The structure was subsequently solved by molecular replacement using the truncated T4 lysozyme (PDB entry 4U15)²⁰ as a search model and refined to R-work = 21.28% and R-free = 24.55% (Table I). We were able to trace the entire polypeptide chain from M1 to L121 [Fig. 1(B)]. Superimposition of the mbT4L and wtT4L proteins revealed that the overall fold of mbT4L originates from the fold of wtT4L with minimal dissimilarities besides truncation of the *N*-terminal lobe [Fig. 1(B)].

The asymmetric unit of the mbT4L/Ni²⁺ crystals contained two molecules of mbT4 lysozyme and four nickel ions [Fig. 1(C)]. Two Ni²⁺ ions formed coordinate covalent bonds with histidines H73, H85, and H89 from the same mbT4L molecule, while the other two Ni²⁺ ions formed coordinate covalent bonds symmetrically with histidines H76 and H80 from one mbT4L molecule and H82 from the other mbT4L molecule from the asymmetric unit, inducing dimerization of mbT4L under conditions within the crystal [Fig. 1(D)].

Next, we analyzed the anomalous scattering from the nickel atoms. We collected a crystallographic dataset at the wavelength of the absorption peak of the nickel atoms (1.4859 Å, Table I). The anomalous scatterers were clearly located at the positions of the nickel atoms [Fig. 1(D)], however, we were not able to solve the entire mbT4L structure using just the anomalous scattering of the nickel atoms and the single-wavelength anomalous dispersion (SAD) technique. Nevertheless, we concluded that co-crystallization of a target mbT4L-fused protein with

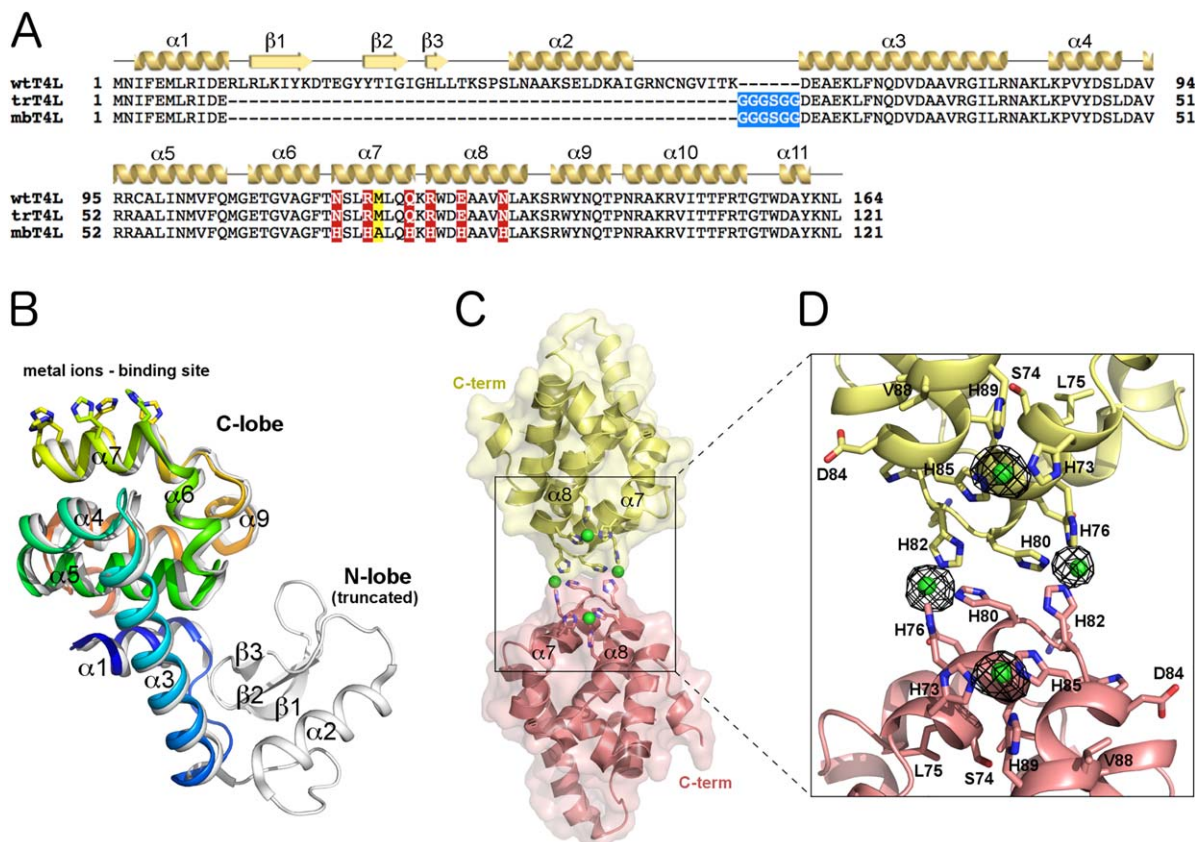


Figure 1. Crystal structure of the metal ions-binding T4 lysozyme. (A) Multiple alignment of the wild-type phage T4 lysozyme (wtT4L), T4 lysozyme with a truncated *N*-terminal lobe as described by Thorsen et al.²⁰ (trT4L), and metal ions-binding T4 lysozyme presented in this study (mbT4L). Blue areas represent the glycine/serine linker (-GGSGG-) replacing the *N*-terminal lobe in trT4L and mbT4L; the red areas represent amino acid residues mutated to histidines in mbT4L, while the yellow area represents the methionine residue mutated to alanine in mbT4L. The numbers indicate amino acids positions. The secondary structures are indicated above the sequences. (B) The overall fold of mbT4L originates from the fold of wtT4L. The protein backbone of mbT4L in cartoon representation is depicted in rainbow colors from blue (*N* terminus) to red (*C* terminus), and is superimposed with wtT4L (PDB entry 3FA0)²¹ depicted in grey. The metal ions-binding site of mbT4L is shown in stick representation. (C) The mbT4L crystals contained two molecules of mbT4L binding four nickel ions per asymmetric unit. The protein backbones in cartoon representation as well as the semi-transparent surfaces of the first and second mbT4L molecule in the asymmetric unit are colored in yellow and red, respectively. The Ni²⁺-binding sites are shown in stick representation. The nickel ions are represented as green spheres. (D) Detailed view of the Ni²⁺-binding sites of the mbT4L molecules in complex with nickel ions depicted as in C. The anomalous scattering was analyzed using a crystallographic dataset at the wavelength of the absorption peak of the nickel atoms (1.4859 Å), and the anomalous map contoured at 3 sigma is shown.

nickel ions may facilitate crystallogenes through formation of the Ni²⁺ ions-dependent crystal contacts of mbT4L. In addition, the molecular replacement/single-wavelength anomalous dispersion (MR-SAD) technique using the mbT4L structure as a search model and the anomalous scattering from the nickel atoms can be applied to solve the crystal structure of this mbT4L-fused protein.

Metal ions-binding T4 lysozyme as an intramolecular protein purification tag

Immobilized-metal affinity chromatography (IMAC) is the most widely used affinity chromatography technique in protein fractionation.²⁴ It is based on the affinity of metal ions such as Co²⁺, Cu²⁺, Ni²⁺, and Zn²⁺ to histidine and cysteine residues and formation of the specific coordinate covalent bonds. The

most important application of IMAC is based on a combination of a tetradentate ligand (such as nitrilotriacetic acid, NTA) ensuring strong immobilization of metal ions such as Ni²⁺ or Co²⁺ that leave two coordination sites free for interaction with biopolymers, and oligohistidine extended (His-tagged) recombinant proteins.

In this section, we investigated utilization of the metal ions-binding T4 lysozyme as an intramolecular protein purification tag in the IMAC technology, and compared its advantages and drawbacks with the commonly used *N*-terminal hexahistidine (His₆) tag. As a model molecule, we choose a chimeric protein composed of the kinase domain of the phosphatidylinositol 4-kinase IIalpha (PI4K2A) and truncated T4 lysozyme. PI4K2A is associated with various cellular membranes through its specific cysteine-rich motif (-LCCPCCF-)

Table I. *Data Collection and Refinement Statistics*

| Dataset | mbT4L/native | mbT4L/anomalous |
|---|---------------------------|---------------------------|
| PDB acc. code | 5I14 | |
| Data collection and processing | | |
| Space group | P 21 21 21 | P 21 21 21 |
| Cell dimensions— <i>a</i> , <i>b</i> , <i>c</i> (Å) | 60.1, 61.2, 69.8 | 60.4, 60.9, 68.9 |
| Cell dimensions— α , β , γ (°) | 90, 90, 90 | 90, 90, 90 |
| Diffraction source | BESSY ID 14-1 | BESSY ID 14-1 |
| Wavelength (Å) | 0.9796 | 1.4859 |
| Resolution range (Å) | 46.02–1.75 (1.81–1.75) | 42.88–2.38 (2.47–2.38) |
| No. of unique reflections | 26668 (2498) | 10526 (942) |
| Mean <i>I</i> / σ (<i>I</i>) | 22.46 (1.33) | 11.24 (2.03) |
| Completeness (%) | 99.45 (95.31) | 99.07 (90.84) |
| Multiplicity | 7.1 (6.7) | 12.1 (12.0) |
| Structure solution and refinement | | |
| R-work (%) | 21.28 (34.06) | 24.31 (31.79) |
| R-free (%) | 24.55 (32.50) | 25.88 (28.87) |
| No. of non-H atoms | 2069 | 1909 |
| R.m.s. deviations—bonds (Å) | 0.006 | 0.003 |
| R.m.s. deviations—angles (°) | 0.94 | 0.91 |
| Average B factors (Å ²) - protein | 36.4 | 49.4 |
| - ligands | 34.8 | 69.0 |
| - solvent | 43.6 | 31.5 |
| Ramachandran favored/outliers (%) | 99/0 | 100/0 |

Statistics for the highest-resolution shell are shown in parentheses.

post-translationally modified with palmitoyl moieties.²⁵ For the purpose of biochemical studies and particularly protein crystallography, this palmitoylated segment of PI4K2A provides a perfect target for replacement with T4 lysozyme. Recently, we successfully employed such T4 lysozyme fusion strategy to facilitate crystallization of both human type II PI4-kinases PI4K2A¹⁵ and its relative PI4K2B.¹⁶

Here, we generated a construct composed of the *N*-terminal His₆ tag followed by a GB1 folding tag and the kinase domain of PI4K2A with the cysteine-rich loop replaced by the truncated T4 lysozyme (His-PI4K2A-trT4L). Next, we generated another construct lacking the *N*-terminal His₆ tag and containing the metal-ions binding T4 lysozyme instead of the truncated T4 lysozyme mutant (PI4K2A-mbT4L) [Fig. 2(A)]. A model of the PI4K2A-mbT4L chimeric protein based on our previously published crystal structure of PI4K2A-wtT4L¹⁵ and the mbT4L crystal structure presented in this study indicates that the metal ions-binding site of mbT4L within the PI4K2A-mbT4L construct can be freely accessed by immobilized metal ions such as NiNTA-immobilized nickel ions as expected [Fig. 2(B)].

Both His-PI4K2A-trT4L and PI4K2A-mbT4L constructs expressed well in *E. coli* with high yields within the range of approximately 10 mg of protein per 1 L of bacterial culture. However, the yields of the PI4K2A-mbT4L chimeric protein were significantly higher than the yields of the His-PI4K2A-trT4L construct [Fig. 2(C)]. Next, we examined the affinity of both His-PI4K2A-trT4L and PI4K2A-

mbT4L chimeric proteins to immobilized nickel ions. Both proteins were sequentially bound to a HisTrap HP (Ni²⁺ Sepharose High Performance) column and eluted with a gradient of imidazole (pH 8.0) ranging from 0 to 400 mM. Elution of these proteins was monitored by the absorbance at 280 nM along with the SDS-PAGE analysis of the collected fractions followed by Coomassie Blue staining [Fig. 2(D)]. The PI4K2A-mbT4L chimeric protein was eluted at significantly higher concentration of imidazole than the His-PI4K2A-trT4L construct, indicating the higher affinity of nickel ions to PI4K2A-mbT4L compared to the affinity to His-PI4K2A-trT4L.

Discussion

Phage T4 lysozyme is a well folded and highly soluble protein which has been used in the fusion protein strategy to facilitate crystallization of various proteins. One of its noteworthy attributes is its tolerance of changes in the amino acid sequence. In this study, we present a structural and biochemical characterization of its novel, metal ions-binding mutant, and investigated its utilization as an intramolecular protein purification tag in the immobilized-metal affinity chromatography.

The metal ions-binding property of this mutant was achieved by introduction of six histidines into the α 7 and α 8 helices of the “minimal version” of T4 lysozyme described by Thorsen et al.²⁰ Structural characterization of the resulting mutant using protein crystallography confirmed that this metal-ions binding mutant of T4 lysozyme (mbT4L) still folds

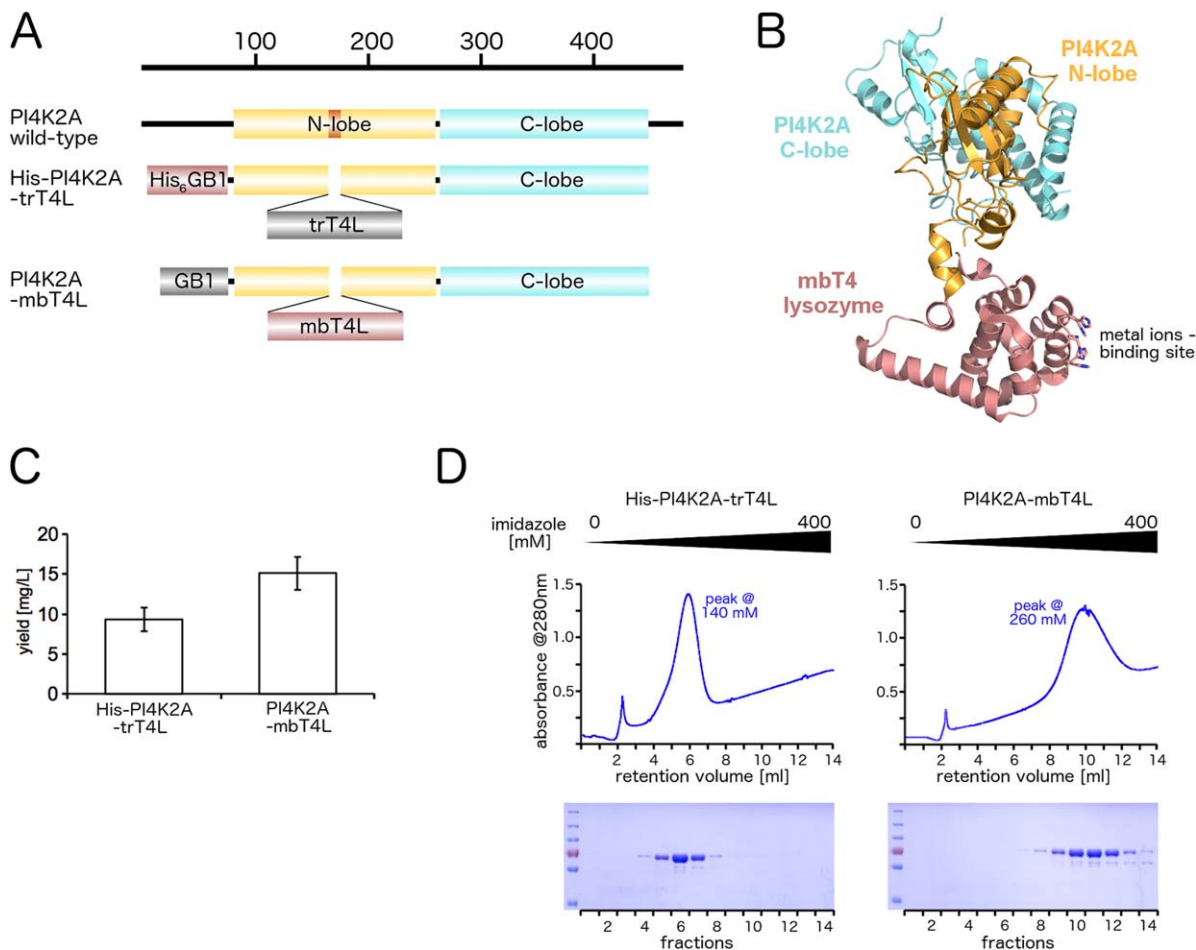


Figure 2. Metal ions-binding T4 lysozyme as an intramolecular protein purification tag. (A) Schematic representation of the wild-type PI4K2A lipid kinase and the chimeric constructs used for further experiments. The *N*-lobe and *C*-lobe of PI4K2A are colored in gold and aquamarine, respectively; the palmitoylated motif of PI4K2A (replaced by T4L in the chimeric constructs) is depicted in orange. The *N*-terminally His₆-tagged GB1 folding tag (His₆GB1) and the metal ions-binding T4 lysozyme (mbT4L) are colored in red, while the GB1 protein lacking the *N*-terminal His₆-tag and the truncated T4 lysozyme lacking the to-histidine mutations (trT4L) are depicted in grey. (B) Model of the PI4K2A-mbT4L chimeric protein based on our previously published crystal structure of the PI4K2A-wtT4L chimeric protein (PDB entry 4PLA)¹⁵ and the mbT4L crystal structure presented in this study. The protein backbone is shown in cartoon representation. The PI4K2A *N*-lobe, *C*-lobe, and mbT4 lysozyme are colored in gold, aquamarine, and red, respectively. The metal ions-binding site of mbT4L is shown in stick representation. (C) Bar graph presents the mean values of the yields of the chimeric proteins from **A** expressed and purified from *E. coli* BL21 (see Materials and methods for more detail); error bars are standard errors of the mean based on three independent experiments. (D) Analysis of the affinity of the chimeric proteins from **A** to immobilized Ni²⁺ ions. Upper panel, elution profiles of the chimeric proteins bound to a HisTrap HP column and eluted with a gradient of imidazole ranging from 0 to 400 mM, monitored by the absorbance at 280 nm. Lower panel, SDS-PAGE analysis of the collected fractions followed by Coomassie Blue staining.

well with minimal dissimilarities compared to the wild-type T4 lysozyme (wtT4L), besides truncation of the *N*-terminal lobe. All six introduced histidines are located at the surface of mbT4L within a small region - the C α atoms of all these residues are located within a region with a radius of approximately 7 Å. Side chains of these residues are solvent accessible and thus capable of binding of metal ions such as Ni²⁺. Within the crystal structure of mbT4L co-crystallized with Ni²⁺ ions, one nickel ion forms coordinate covalent bonds with three histidines of mbT4L. However, in case of mbT4L bound to NTA-

immobilized Ni²⁺ ions we expect a stoichiometry of one nickel ion per two histidines of mbT4L, given the tetravalency of the nitrilotriacetic acid leaving two Ni²⁺ coordination sites free for interaction with the mbT4L histidines.

Oligohistidine tags are common tools for purification of recombinant proteins expressed in *E. coli* or other prokaryotic expression systems by the IMAC technique. In this study, we compared utilization of the commonly used *N*-terminal hexahistidine tag with application of an intramolecular fusion of the target protein with the mbT4 lysozyme.

Intramolecular mbT4L fusion may provide several advantages compared to the *N*-terminal His₆-tag or compared to the intramolecular wtT4L fusion as follows:

- MbT4L is not affected by degradation of the intrinsically disordered *N* terminus of the target mbT4L-fused protein by *N*-terminal peptidases. This implies that knowledge of exact domain boundaries for the expression of the target protein in a prokaryotic expression system is not essential. Negligible degradation of the purification tag also contributes to higher yields of the purified protein.
- MbT4L-fusion improves the solubility of the target protein.
- Target mbT4-fused protein binds to the immobilized metal ions with stronger affinity than the His₆-tagged protein, resulting in its higher purity upon purification by the IMAC technique.
- Co-crystallization of a target mbT4L-fused protein with metal ions may facilitate crystallogenesi through formation of specific metal ions-dependent crystal contacts of mbT4L.
- MR-SAD technique using the mbT4L structure as a search model and the anomalous scattering from the metal atoms can be applied to solve the crystal structure of a target mbT4L-fused protein.

In case that a high concentration of imidazole (or its basic pH) is disadvantageous for the target protein, the imidazole concentration during elution can be modulated by pH of the elution buffer, salt concentration, addition of EDTA or other chelating agents, etc., similarly as in case of elution of the *N*-terminally histidine-tagged proteins.^{24,26}

The obvious practical drawback of utilization of the intramolecular mbT4L fusion, similarly to the intramolecular wtT4L fusion, is the right positioning of mbT4L within the target protein, especially in case when the structure of the target protein (or its homologue) is not known and is difficult to predict. In addition, even in case that the lysozyme position appropriate for protein expression and purification is achieved (such as within the palmitoylated loop of type II PI4-kinases^{15,16} or within the third intracellular loop of multiple G protein-coupled receptors²⁰), generation of tens of mutants with slightly shifted lysozyme positions is usually required to achieve crystallization.

In summary, we designed a novel, metal ions-binding mutant of phage T4 lysozyme and presented its high resolution crystal structure in complex with Ni²⁺ ions. Our study provides a structural rationale and methodological insights for its utilization as an intramolecular protein purification tag for purification of recombinant proteins by the IMAC technique.

Materials and Methods

Plasmids

Wild-type phage T4 lysozyme was cloned into *Nde*I and *Kpn*I restriction sites of the pRSFD vector (Novagen) using routine restriction cloning. Truncated and metal ions-binding T4L mutants were generated using the Phusion Site-Directed Mutagenesis Kit (Thermo Scientific). Human PI4K2A residues 76–467 with a palmitoylation motif replaced by wtT4L was cloned into pRSFD vector with an *N*-terminal His₆-tag followed by a GB1 folding tag as described previously¹⁵ and further mutated using the Phusion Site-Directed Mutagenesis Kit. All DNA constructs were verified by sequencing.

Protein expression and purification

Metal ions-binding T4 lysozyme and PI4K2A-T4L chimeric proteins were expressed in *E. coli* BL21 Star cells using the ZY5052 autoinduction medium. The bacterial cells were grown at 37°C to OD600 of 0.7 and then cultivated at 18°C for another 20 h. Then, they were harvested by centrifugation and lysed in the lysis buffer (50 mM Tris, 300 mM NaCl, 3 mM β-mercaptoethanol, 30 mM imidazole, 10% glycerol, pH 8.0). The lysate was incubated with the Ni-NTA resin (Macherey-Nagel) and then extensively washed with the lysis buffer. The protein was eluted with the lysis buffer supplemented with 300 mM imidazole (pH 8.0). The proteins were further purified using the size exclusion chromatography at Superdex 75 or Superdex 200 columns (GE Healthcare) in the SEC buffer (10 mM Tris, 200 mM NaCl, 3 mM β-ME, pH 8.0). The molecular weight and purity of all proteins was verified by SDS-PAGE and Matrix-Assisted Laser Desorption/Ionisation (MALDI). Purified proteins were concentrated, aliquoted, flash frozen in the liquid nitrogen, and stored at –80°C until needed.

Crystallization and data collection

Crystals were grown at 20°C in a sitting drop consisting of a 1:1 mixture of the protein supplemented with 2mM NiCl₂ and a well solution (20% PEG 6000, 100 mM MES pH 5). The crystals were cryoprotected in the well solution supplemented with 20% glycerol, flash frozen in the liquid nitrogen, and analyzed. Measurements were carried out at the synchrotron BESSY II (MX14.1 beamline) at Helmholtz-Zentrum Berlin.²⁷ The crystallographic datasets were collected from single frozen crystals.

Structure determination and refinement

The crystallographic data were integrated and scaled using *XDS*.²⁸ The structure of the metal ions-binding T4 lysozyme was solved by molecular replacement using the truncated T4 lysozyme (PDB entry 4U15)²⁰ as a search model. The initial MR

model was obtained with *Phaser*²⁹ from the *Phenix* package.³⁰ The model was further improved using automatic model refinement with *Phenix.refine*³¹ and manual model building with *Coot*.³² Structural figures were generated with *PyMol*.³³

Data Deposition

Coordinates and structure factors of the metal ion-binding T4 lysozyme presented in this study have been submitted to the Protein Data Bank (www.pdb.org) and assigned the identifier 5I14.

Acknowledgments

We thank Helmholtz-Zentrum Berlin for the allocation of synchrotron radiation beam time.

Conflict of Interest

The authors declare no conflict of interest.

References

1. Young I, Wang I, Roof WD (2000) Phages will out: strategies of host cell lysis. *Trends Microbiol* 8:120–128.
2. Baase WA, Liu L, Tronrud DE, Matthews BW (2010) Lessons from the lysozyme of phage T4. *Protein Sci* 19:631–641.
3. Chien EY, Liu W, Zhao Q, Katritch V, Han GW, Hanson MA, Shi L, Newman AH, Javitch JA, Cherezov V, Stevens RC (2010) Structure of the human dopamine D3 receptor in complex with a D2/D3 selective antagonist. *Science* 330:1091–1095.
4. Granier S, Manglik A, Kruse AC, Kobilka TS, Thian FS, Weis WI, Kobilka BK (2012) Structure of the delta-opioid receptor bound to naltrindole. *Nature* 485:400–404.
5. Haga K, Kruse AC, Asada H, Yurugi-Kobayashi T, Shiroishi M, Zhang C, Weis WI, Okada T, Kobilka BK, Haga T, Kobayashi T (2012) Structure of the human M2 muscarinic acetylcholine receptor bound to an antagonist. *Nature* 482:547–551.
6. Jaakola VP, Griffith MT, Hanson MA, Cherezov V, Chien EY, Lane JR, Ijzerman AP, Stevens RC (2008) The 2.6 angstrom crystal structure of a human A2A adenosine receptor bound to an antagonist. *Science* 322:1211–1217.
7. Kruse AC, Hu J, Pan AC, Arlow DH, Rosenbaum DM, Rosemond E, Green HF, Liu T, Chae PS, Dror RO, Shaw DE, Weis WI, Wess J, Kobilka BK (2012) Structure and dynamics of the M3 muscarinic acetylcholine receptor. *Nature* 482:552–556.
8. Manglik A, Kruse AC, Kobilka TS, Thian FS, Mathiesen JM, Sunahara RK, Pardo L, Weis WI, Kobilka BK, Granier S (2012) Crystal structure of the micro-opioid receptor bound to a morphinan antagonist. *Nature* 485:321–326.
9. Rosenbaum DM, Cherezov V, Hanson MA, Rasmussen SG, Thian FS, Kobilka TS, Choi HJ, Yao XJ, Weis WI, Stevens RC, Kobilka BK (2007) GPCR engineering yields high-resolution structural insights into beta2-adrenergic receptor function. *Science* 318:1266–1273.
10. Shimamura T, Shiroishi M, Weyand S, Tsujimoto H, Winter G, Katritch V, Abagyan R, Cherezov V, Liu W, Han GW, Kobayashi T, Stevens RC, Iwata S (2011)

Structure of the human histamine H1 receptor complex with doxepin. *Nature* 475:65–70.

11. Wu B, Chien EY, Mol CD, Fenalti G, Liu W, Katritch V, Abagyan R, Brooun A, Wells P, Bi FC, Hamel DJ, Kuhn P, Handel TM, Cherezov V, Stevens RC (2010) Structures of the CXCR4 chemokine GPCR with small-molecule and cyclic peptide antagonists. *Science* 330:1066–1071.
12. Zhang C, Srinivasan Y, Arlow DH, Fung JJ, Palmer D, Zheng Y, Green HF, Pandey A, Dror RO, Shaw DE, Weis WI, Coughlin SR, Kobilka BK (2012) High-resolution crystal structure of human protease-activated receptor 1. *Nature* 492:387–392.
13. Tong J, Yang H, Yang H, Eom SH, Im YJ (2013) Structure of Osh3 reveals a conserved mode of phosphoinositide binding in oxysterol-binding proteins. *Structure* 21:1203–1213.
14. Yang H, Tong J, Lee CW, Ha S, Eom SH, Im YJ (2015) Structural mechanism of ergosterol regulation by fungal sterol transcription factor Upc2. *Nat Commun* 6:6129.
15. Baumlova A, Chalupska D, Rozycki B, Jovic M, Wisniewski E, Klima M, Dubankova A, Kloer DP, Nencka R, Balla T, Boura E (2014) The crystal structure of the phosphatidylinositol 4-kinase II. *EMBO Rep* 15:1085–1092.
16. Klima M, Baumlova A, Chalupska D, Hřebabeký H, Dejmek M, Nencka R, Boura E (2015) The high-resolution crystal structure of phosphatidylinositol 4-kinase II β and the crystal structure of phosphatidylinositol 4-kinase II α containing a nucleoside analogue provide a structural basis for isoform-specific inhibitor design. *Acta Cryst D* 71:1555–1563.
17. Baumlova A, Gregor J, Boura E (2016) The structural basis for calcium inhibition of lipid kinase PI4K II α and comparison with the apo state. *Physiol Res* 65:987–993.
18. Zou Y, Weis WI, Kobilka BK (2012) N-terminal T4 lysozyme fusion facilitates crystallization of a G protein coupled receptor. *PLoS One* 7:e46039.
19. Rennell D, Bouvier SE, Hardy LW, Poteete AR (1991) Systematic mutation of bacteriophage T4 lysozyme. *J Mol Biol* 222:67–88.
20. Thorsen TS, Matt R, Weis WI, Kobilka BK (2014) Modified T4 lysozyme fusion proteins facilitate G protein-coupled receptor crystallogenesis. *Structure* 22:1657–1664.
21. Mooers BH, Tronrud DE, Matthews BW (2009) Evaluation at atomic resolution of the role of strain in destabilizing the temperature-sensitive T4 lysozyme mutant Arg 96 \rightarrow His. *Protein Sci* 18:863–870.
22. Matthews BW, Remington SJ, Grutter MG, Anderson WF (1981) Relation between hen egg white lysozyme and bacteriophage T4 lysozyme: evolutionary implications. *J Mol Biol* 147:545–558.
23. Matsumura M, Matthews BW (1989) Control of enzyme activity by an engineered disulfide bond. *Science* 243:792–794.
24. Block H, Maertens B, Spriestersbach A, Brinker N, Kubicek J, Fabis R, Labahn J, Schafer F (2009) Immobilized-metal affinity chromatography (IMAC): a review. *Methods Enzymol* 463:439–473.
25. Boura E, Nencka R (2015) Phosphatidylinositol 4-kinases: Function, structure, and inhibition. *Exper Cell Res* 337:136–145.
26. Bornhorst JA, Falke JJ (2000) Purification of proteins using polyhistidine affinity tags. *Methods Enzymol* 326:245–254.

27. Mueller U, Darowski N, Fuchs MR, Förster R, Hellmig M, Paithankar KS, Pühringer S, Steffien M, Zocher G, Weiss MS (2012) Facilities for macromolecular crystallography at the Helmholtz-Zentrum Berlin. *J Synch Radiat* 19:442–449.
28. Kabsch W (2010) XDS. *Acta Cryst D* 66:125–132.
29. McCoy AJ, Grosse-Kunstleve RW, Adams PD, Winn MD, Storoni LC, Read RJ (2007) Phaser crystallographic software. *J Appl Cryst* 40:658–674.
30. Adams PD, Afonine PV, Bunkóczi G, Chen VB, Davis IW, Echols N, Headd JJ, Hung L-W, Kapral GJ, Grosse-Kunstleve RW, McCoy AJ, Moriarty NW, Oeffner R, Read RJ, Richardson DC, Richardson JS, Terwilliger TC, Zwart PH (2010) PHENIX: a comprehensive Python-based system for macromolecular structure solution. *Acta Cryst D* 66:213–221.
31. Afonine PV, Grosse-Kunstleve RW, Echols N, Headd JJ, Moriarty NW, Mustyakimov M, Terwilliger TC, Urzhumtsev A, Zwart PH, Adams PD (2012) Towards automated crystallographic structure refinement with phenix.refine. *Acta Cryst D* 68:352–367.
32. Emsley P, Cowtan K (2004) Coot: model-building tools for molecular graphics. *Acta Cryst D* 60:2126–2132.
33. Schrodinger (2015) The PyMOL Molecular Graphics System, Version 1.8. In